Collimation of Energetic Electrons from a Laser-Target Interaction by a Magnetized Target Back Plasma Preformed by a Long-Pulse Laser

H. B. Zhuo,[1,*] Z. L. Chen,[2] Z. M. Sheng,[3,4] M. Chen,[3] T. Yabuuchi,[5] M. Tampo,[5] M. Y. Yu,[6,7] X. H. Yang,[1] C. T. Zhou,[1,8] K. A. Tanaka,[2,5] J. Zhang,[3] and R. Kodama[2,5]

[1]*College of Science, National University of Defense Technology, Changsha 410073, People's Republic of China*
[2]*Graduate School of Engineering, Osaka University 2-1 Yamada-oka, Suita, Osaka 565-0871, Japan*
[3]*MOE Key Laboratory for Laser Plasmas and Department of Physics and Astronomy, Shanghai Jiao Tong University, Shanghai 200240, People's Republic of China*
[4]*Department of Physics, SUPA, University of Strathclyde, Glasgow G4 0NG, United Kingdom*
[5]*Institute of Laser Engineering, Osaka University 2-6 Yamada-oka, Suita, Osaka 565-0871, Japan*
[6]*Institute for Fusion Theory and Simulation and Department of Physics, Zhejiang University, Hangzhou 310027, People's Republic of China*
[7]*Institute for Theoretical Physics I, Ruhr University, Bochum D-44780, Germany*
[8]*Institute of Applied Physics and Computational Mathematics, Beijing 100094, People's Republic of China*

It is demonstrated experimentally and by numerical simulations that the presence of a long-pulse-laser-created back plasma on the target backside can focus the relativistic electrons produced by short-pulse laser interaction with the front of a solid target. Comparing this to that without the back plasma, the number density of the fast electrons is increased by one order of magnitude, and their divergence angle is reduced fivefold. The effect is attributed to the absence of the backside sheath electric field and the collimation effect of the megagauss self-generated baroclinic magnetic field there. Such an acceleration scheme can be useful to applications requiring high-energy and charge-density electron bunches, such as fast ignition in inertial fusion.

Energetic electron (EE) bunches are useful for fast ignition in inertial fusion [1–4], realization of high-energy density states [5], compact particle accelerators [6], and novel radiation sources [7], as well as in medical therapy [8]. Fast ignition, for example, demands electron energy deposition at the kilojoule level inside the fuel pellet core [1]. EE bunches produced in intense short-pulse laser-solid target interaction can have fairly high number (10^{14}), charge (10 μC), and energy (several tens joules) [9,10]. However, they also have a large divergence angle θ_d ($\sim 30° - 50°$). It is thus essential to reduce the spatial spread of the EEs for practical applications.

Collimation of EEs by the intense magnetic fields induced by their return currents has been proposed [11] and investigated extensively for different target designs [12,13]. Using a prepulse to produce an azimuthal magnetic field can also reduce the fast-electron divergence and increase the electron current density [14,15]. On the other hand, due to the ubiquitous presence of orthogonal density and temperature gradients, multimegagauss magnetic fields are easily generated baroclinically in the plasma created by a long-pulse laser interacting with a target [16–18]. The baroclinic magnetic field (BMF) is given by $\partial_t \boldsymbol{B} = \nabla T_e \times \nabla n_e / n_e e$, where t is the time, $\boldsymbol{B}$ is the magnetic field, e, n_e, and T_e are electron charge, density and temperature, respectively. The BMF is on a much longer time scale (few hundred ps) than

that (few tens fs) of the EEs generated by intense short laser pulses.

In this Letter, we show that in the presence of a magnetized plasma pregenerated by a long-pulse laser impinging the backside of the target, the intrinsically divergent EEs that have passed through the target can be collimated by the toroidal BMF. The backside plasma also allows the EEs to propagate more stably and suppresses the target normal sheath electric field there by neutralizing the less energetic hot electrons from the target front. As a result, a tight EE bunch with high energy and charge densities can be produced. The proposed process is schematically illustrated and discussed in Fig. 1(a).

To bend the trajectory of a fast electron of speed v at an angle θ_d with respect to the axial (z) direction, the magnetic field should satisfy [14]

$$B_\phi L_r \geq \frac{\gamma v m_e}{e} S, \qquad (1)$$

where m_e is electron mass, L_r is the scale length of the transverse (r-direction) magnetic field, $\gamma = (1 - v^2/c^2)^{-1/2}$ is the Lorentz factor, and $S = 1 - \cos(\theta_d/2)$. For a fast electron generated at the front side of the target by the main laser pulse of intensity I_0 and wavelength λ_0, the factor γv is determined by the corresponding ponderomotive force [19]. Accordingly, the condition for
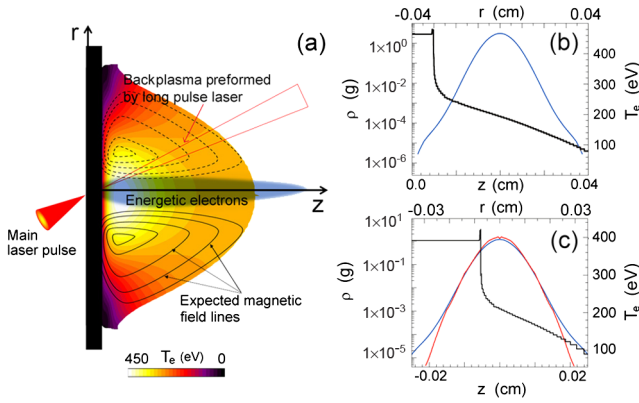
FIG. 1 (color online). (a) Schematic representation of the target backside plasma. The electron temperature distribution is drawn basing on the results (at 400 ps) from hydrodynamic simulations of the interaction of a long-pulse laser with the backside of a planar Al target. The contours (thin black closed curves) depict the expected toroidal baroclinic magnetic field, which is peaked around the edge of the laser focal spot and decreases to zero on the axis ($r = 0$) and at large distances from the focal spot. The EEs (blue region) created and accelerated by the target front laser are focused into a narrow bunch by the strong magnetic field. The hydrodynamic simulation results for the back plasma electron density (black) along the z axis, and temperature (blue) along the r at the position of 0.01 cm away from rear surface of the target, are shown in (b) for the Al target with flat backside, and (c) for two plastic targets with different backside curvatures (blue: infinite, and red: 2.5 mm).

deflecting the divergent electron towards the axial direction can be written as [14]

$$B_\phi L_r \geq \frac{m_e c}{e} \sqrt{1 + \frac{I_0 \lambda_0^2}{1.38 \times 10^{18} \text{ W cm}^{-2} \mu\text{m}^2} S}, \quad (2)$$

where c is vacuum light speed.

We use the radiative hydrodynamics code MULTI2D [20] to simulate the laser-excited plasma expansion and magnetic field generation at the target backside. In accordance with our experimental parameters, a 2 J p-polarized 1.053 μm 400 ps long laser pulse is focused on a 50 μm-thick Al target with a $\sim$300 μm spot diameter. Figure 1(b) shows that the electron density gradient is mainly in the axial direction, as expected. That is, the axial temperature gradient does not contribute to the BMF generation. The magnitude of the BMF can then be roughly given by $B_0 \sim T_e t / l_n l_T$, where l_n and l_T are the scale lengths of the density and temperature, respectively. For $T_e \sim 400$ eV, $l_n \sim 10$ μm, and $l_T \sim 150$ μm [estimated from Fig. 1(b)], we find that the magnetic field attains 1 MG in 400 ps. For 200 μm-thick plastic targets with different target back curvatures, our simulations show almost no difference in the axial profiles of the plasma

density. On the other hand, the radial temperature gradient increases with the curvature since the plasma is transversely better confined, as shown in Fig. 1(c). Accordingly, with a $\sim$1 MG BMF in the back plasma of $L_r \sim 150$ μm, the collimation condition (2) is readily satisfied for EEs driven by a $I_0 \lambda_0^2 = 5 \times 10^{18}$ W cm^{-2} μm^2 main laser pulse and exiting the target back with $\theta_d \sim 50°$.

Collimation of the EEs in the intense laser interaction at the target front are tested for both planar Al targets and plastic targets with concave back surfaces on the GEKKO Module II laser system at the Institute of Laser Engineering, Osaka University. The experimental setup is shown in Fig. 2(a). After a 400 ps delay for the preplasma driven by a long-pulse laser at the target back surface to form, EEs are generated at the target front surface by a p-polarized 10 J 1.053 μm 0.6 ps short-pulse laser at a 20° incident angle. The laser pulse is focused by an $f/3.8$ off-axis parabolic mirror into a 20 μm diameter spot with peak intensity $\sim$5 $\times$ 10^{18} W cm^{-2}. To probe the energy-resolved angular distribution of the EEs along the axis of the main laser, a sandwich detector is placed $\sim$4 cm away from the target back. It consists of four layers of photostimulated luminescence (PSL) imaging plates (IPs) with in-between copper filters for detecting 0.4, 3, 6, and 10 MeV electrons. A radiochromic film (RCF) layer and a CR-39 layer in front of the IPs are used to monitor the angular distribution of energetic protons. A 10 μm-thick Al foil is placed in front of the detectors to shield them from the target debris. The entire detector system is wrapped with black tapes and Al foils to block stray light. Tests showed that the small
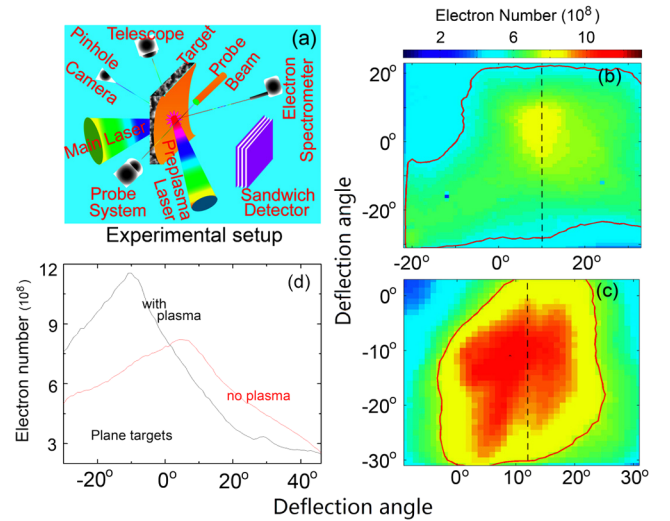

FIG. 2 (color online). Experimental setup (a). Observed angular distribution of electrons over 0.4 MeV for planar Al target with (b) and without (c) preformed plasma on the backside. The p-polarized main laser pulse defining the angular direction (0°, 0°) is incident obliquely at a 20° angle on the front surface of the target (such that the target normal is in the (20°, 0°) direction. (d) Number of > 0.4 MeV electrons along the gray dashed lines in the panels (b) and (c).

number of protons from target normal sheath acceleration can be completely stopped from arriving at the IPs by the RCF and CR-39 layers.

The angular distribution of the EEs behind a plain Al target without a preformed back plasma is shown in Fig. 2(b). We see that the electrons are of low density (8×10^8) and have a rather irregular average angular spread of more than $50°$ around the laser axis at $0°$. Figure 2(c) shows that, in the presence of a performed plasma behind the target, the electrons are much more uniform and of much higher density (1.2×10^9). They are also much better collimated, with the average angular spread reduced to $\sim 30°$. It should be mentioned that despite their near axial direction and narrow spread, the mean direction of the EEs varies somewhat from shot to shot, which can be attributed to uncertainties in the configuration (which determines the focusing direction) of the self-generated magnetic field.

In order to see in more detail the effect of the back plasma and the self-generated magnetic field, we have also considered plastic targets with different concave back surfaces. As discussed, the latter determines the back plasma density and temperature as well as their gradients, and therefore also the self-generated BMF. The results are shown in Fig. 3. One can see that as the curvature radius is reduced from infinite (a) to 5 mm (b) to 2.5 mm (c), the spatial spread of the EEs becomes smaller and their number density higher. Similar to that for the flat Al target, the
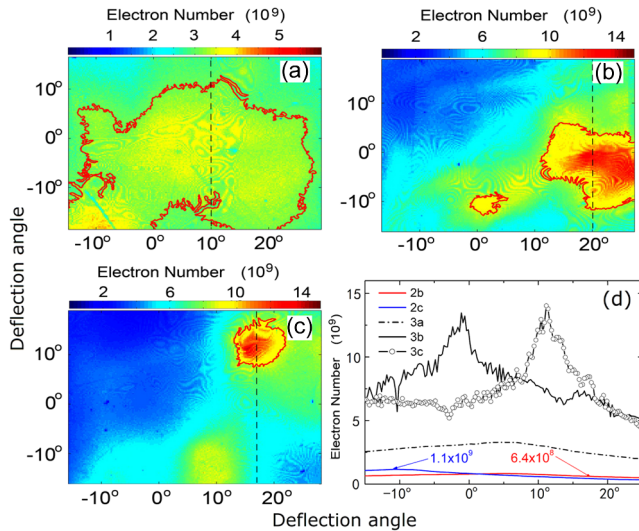

FIG. 3 (color online). Experimental angular distributions of energetic electrons over 0.4 MeV for different cylindrical target back curvatures: (a) infinite (or planar), (b) 5.0 mm, and (c) 2.5 mm, for 200 μm × (5 × 5 mm^2) plastic targets. The curvature axes in (b) and (c) are perpendicular and parallel, respectively, to the laser polarization. (d) Electron number (obtained from the sandwich detector using photo stimulated luminescence) along the dashed lines in Figs. 2(b), 2(c), 3(a), 3(b), and 3(c), denoted by 2b, 2c, 3a, 3b, and 3c, respectively.

deviation of the EEs from the exact axial direction of the main laser is due to uncertainty in the configuration of the baroclinic magnetic field.

For comparison, Fig. 3(d) shows the electron number along the dashed lines in Figs. 2(b) and 2(c) and 3(a)–3(c) for the five cases. We see that the electrons behind the curved-back target are much better collimated. Their number is also more than one order of magnitude higher than that behind the flatback target. These results represent a significant improvement over that of the exiting experiments [21]. In fact, Figs. 3(a) and 3(c) show that the divergence of the EEs is reduced from about $\theta_d \sim 30°$ for the flatback target to about $\theta_d \sim 10°$ for the curved-back target. Moreover, the number density in the center region is increased fivefold. We note that if all the EEs in the original $30°$ divergence angle were focused into the $10°$ divergence angle, the density enhancement factor would be ~ 9.5, which is larger than the experimental value ~ 5.0. The discrepancy can be attributed to filamentation [22,23] of the fast EEs as they propagate in the underdense region of the back plasma. As can be seen in Figs. 3(b) and 3(c), some electrons are scattered away from the EE bunch.

To further clarify the collimation effect of the BMF as observed in our experiments, we have carried out two-dimensional simulations of the process using the particle-in-cell (PIC) simulation code PDLPICC2D [6]. A 3.425×10^{19} W/cm^2 laser pulse of 100 laser cycles in FWHM is focused to a $10\lambda_0$-diameter spot on a 5 μm-thick solid density ($n_0 = 20n_c$) plasma slab at $x = 5$ μm. The preformed back plasma is modeled by an exponentially decaying plasma, with density $n_0 \exp[-(x-10)/10]$cm^{-3}, attached to the back of the target. The model BMF is given by $\boldsymbol{B} = 2B_0(y - 0.5L_y)\boldsymbol{e}_z/L_y$, where $L_y = 128$ μm is the height of the simulation box. Figure 4 shows the distributions of the magnetic fields (left column) and > 1 MeV EEs (center and right columns) for $B_0 = 0$, 5, and 10 MG, corresponding to the collimation condition (2) not satisfied, satisfied, and well satisfied, respectively. Note that the magnetic fields associated with the front laser and the filamentation of the EEs are much stronger and much more localized than the model BMF [the large red and blue shaded areas in Figs. 4(d) and 4(g)] behind the target. However, these intense fields are not directly of our interest here.

In Fig. 4 we can see that filamentation of the EEs occurs as they exit the rear side of the target, and in the absence of the BMF the filaments, together with their induced magnetic fields, are highly divergent. As B_0 increases, the electron filaments, or the electron jets as a whole, become better collimated and focused, even though locally they appear to be unstable to kink- or sausagelike instabilities and tend to breakup and then coalesce into larger filaments, as can be seen in Fig. 4, right column, for the EE density at $x = 30$ μm. We can also see that, because of much improved focusing, the peak EE number density is
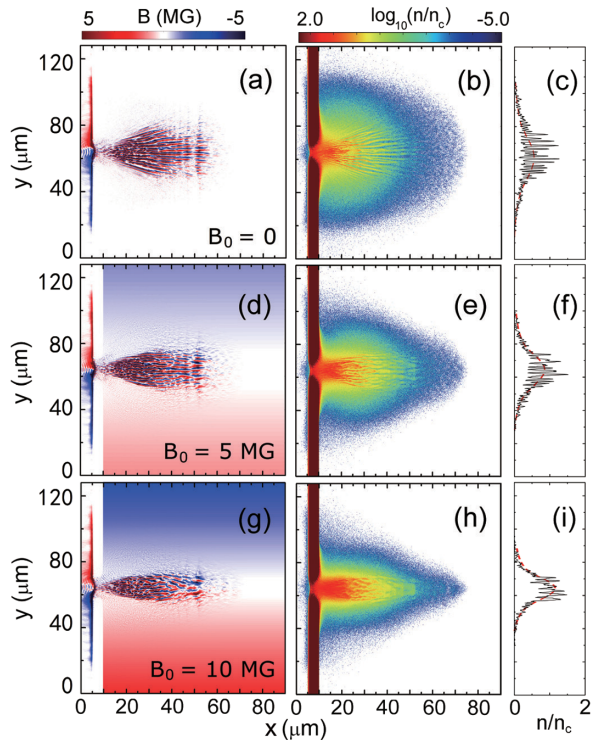
FIG. 4 (color online). Results from two-dimensional PIC simulations at $t = 80$ laser periods from the laser impact: magnetic field distribution (left column), distribution of > 1 MV energetic electrons (center column), and electron density at $x = 30$ μm (right column), for $B_0 = 0$ MG (top row), $B_0 = 5$ MG (center row), and $B_0 = 10$ MG (bottom row). The 5 μm-thick solid-density ($20n_c$, where $n_c = 1.1 \times 10^{21}/\text{cm}^3$) target is at $5 < x[\mu\text{m}] < 10$. Note that the magnetic fields associated with the front-laser interaction with the target and the energetic-electron filamentation are much stronger and localized than the baroclinic magnetic fields, shown in (d) and (g) as large blue and red lightly shaded regions, in the model back plasma.

enhanced by a factor of about 4 as B_0 increases from 0 to 10 MG. Except for the precise location (unpredictable in the experiments) of the peaks, these simulation results agree qualitatively well with that [Fig. 3(d)] from the experiments.

In summary, focusing of intense short-pulse laser generated EEs from the front of a solid target by the BMF in a back plasma precreated at the target backside by a long-pulse laser is demonstrated experimentally and by PIC simulation. The EEs, originally having a large divergence angle ($\theta_d \sim 50°$), are collimated into a tight bunch with $\theta_d \sim 10°$ as they propagate in the back plasma. The focusing and collimation effects are attributed to the strong BMF generated by the nonparallel density and temperature gradients in the back plasma. The results from our analytical estimate and the PIC simulation agree reasonably well with that from the experiment. The proposed scheme provides a simple and effective method for collimating a

large number of initially highly divergent EEs, such that an electron bunch of high-energy and -charge densities can be produced.

*hongbin.zhuo@gmail.com
[1] M. Tabak, J. Hammer, M. E. Glinsky, W. L. Kruer, S. C. Wilks, J. Woodworth, E. M. Campbell, M. D. Perry, and R. J. Mason, Phys. Plasmas **1**, 1626 (1994).
[2] M. Tabak, D. S. Clark, S. P. Hatchett, M. H. Key, B. F. Lasinski, R. A. Snavely, S. C. Wilks, R. P. J. Town, R. Stephens, E. M. Campbell, R. Kodama, K. Mima, K. A. Tanaka, S. Atzeni, and R. Freeman, Phys. Plasmas **12**, 057305 (2005).
[3] R. Kodama, P. A. Norreys, K. Mima, A. E. Dangor, R. G. Evans, H. Fujita, Y. Kitagawa, K. Krushelnick, T. Miyakoshi, N. Miyanaga, T. Norimatsu, S. J. Rose, T. Shozaki, K. Shigemori, A. Sunahara, M. Tampo, K. A. Tanaka, Y. Toyama, T. Yamanaka, and M. Zepf, Nature (London) **412**, 798 (2001).
[4] R. Kodama et al., Nature (London) **418**, 933 (2002).
[5] R. Kodama et al., Nature (London) **432**, 1005 (2004).
[6] H. B. Zhuo, Z. L. Chen, W. Yu, Z. M. Sheng, M. Y. Yu, Z. Jin, and R. Kodama, Phys. Rev. Lett. **105**, 065003 (2010).
[7] Z. Jin, Z. L. Chen, H. B. Zhuo, A. Kon, M. Nakatsutsumi, H. B. Wang, B. H. Zhang, Y. Q. Gu, Y. C. Wu, B. Zhu, L. Wang, M. Y. Yu, Z. M. Sheng, and R. Kodama, Phys. Rev. Lett. **107**, 265003 (2011).
[8] S. V Bulanov, T. Zh Esirkepov, V. S Khoroshkov, A. V Kuznetsov, and F. Pegoraro, Phys. Lett. A **299**, 240 (2002).
[9] J. S. Green et al., Phys. Rev. Lett. **100**, 015003 (2008).
[10] K. L. Lancaster, J. S. Green, D. S. Hey, K. U. Akli, J. R. Davies, R. J. Clarke, R. R. Freeman, H. Habara, M. H. Key, R. Kodama, K. Krushelnick, C. D. Murphy, M. Nakatsutsumi, P. Simpson, R. Stephens, C. Stoeckl, T. Yabuuchi, M. Zepf, and P. A. Norreys, Phys. Rev. Lett. **98**, 125002 (2007).
[11] A. R. Bell and R. J. Kingham, Phys. Rev. Lett. **91**, 035003 (2003).
[12] A. P. L. Robinson and M. Sherlock, Phys. Plasmas **14**, 083105 (2007).
[13] S. Kar, A. P. L. Robinson, D. C Carroll, O. Lundh, K. Markey, P. McKenna, P. Norreys, and M. Zepf, Phys. Rev. Lett. **102**, 055001 (2009).
[14] A. P. L. Robinson, M. Sherlock and P. A. Norreys, Phys. Rev. Lett. **100**, 025002 (2008).
[15] R. H. H. Scott et al., Phys. Rev. Lett. **109**, 015001 (2012).
[16] J. A. Stamper, K. Papadopoulos, R. N. Sudan, S. O. Dean, and E. A. McLean, Phys. Rev. Lett. **26**, 1012 (1971).

[17] O. Willi, P. T. Rumsby, and C. Duncan, Opt. Commun. **37,** 40 (1981).

[18] M. Borghesi, A. J. MacKinnon, A. R. Bell, R. Gaillard, and O. Willi, Phys. Rev. Lett. **81,** 112 (1998).

[19] S. C. Wilks and W. L. Kruer, IEEE J. Quantum Electron. **33,** 1954 (1997).

[20] R. Remis, R. Schmaltz and J. Meyer-Ter-Vehn, Comput. Phys. Commun. **49,** 475 (1988).

[21] T. Yabuuchi, K. Adumi, H. Habara, R. Kodama, K. Kondo, T. Tanimoto, K. A. Tanaka, Y. Sentoku, T. Matsuoka, Z. L. Chen, M. Tampo, A. L. Lei and K. Mima, Phys. Plasmas **14,** 040706 (2007).

[22] M. Tatarakis, F. N. Beg, E. L. Clark, A. E. Dangor, R. D. Edwards, R. G. Evans, T. J. Goldsack, K. W. D. Ledingham, P. A. Norreys, M. A. Sinclair, M. S. Wei, M. Zepf, and K. Krushelnick, Phys. Rev. Lett. **90,** 175001 (2003).

[23] M. S. Wei, F. N. Beg, E. L. Clark, A. E. Dangor, R. G. Evans, A. Gopal, K. W. D. Ledingham, P. McKenna, P. A. Norreys, M. Tatarakis, M. Zepf, and K. Krushelnick, Phys. Rev. E **70,** 056412 (2004).